200 kA DC Busbar Demonstrator DEMO 200 – Conceptual Design of Superconducting 20 kA Busbar Modules made of HTS CroCo Strands

Michael J. Wolf, Walter H. Fietz, *Senior Member*, *IEEE*, Mathias Heiduk, Stefan Huwer, Andreas Kienzler, Sonja I. Schlachter, Thomas Vogel

***Abstract*— The High Temperature Superconductor (HTS) material REBCO provides high critical currents even when being cooled with liquid nitrogen (LN_2) to T ~ 70-77 K. Therefore, it is considered in the design of energy-efficient superconducting busbar solutions for industrial high-current application such as electrolysis. The research project DEMO 200 aims to demonstrate a modular, superconducting, LN_2-cooled 200 kA DC busbar for an aluminum electrolysis plant.**

Within that project, the electromagnetic design and analysis of a round arrangement of twelve individual compact HTS CrossConductor (HTS CroCo) strands is carried out. The HTS CroCo strands are fabricated from REBCO tapes of 2 mm and 3 mm width. For the electromagnetic design of the modules and busbar, the angular field dependence of the critical current of the REBCO material was characterized at relevant temperature and field ranges. The data is used as an input for an electromagnetic model to determine the required amount of REBCO to achieve the target critical current in the modular 200 kA busbar. For a sub-scale test of one module at T = 77 K, the expected critical currents are calculated to allow for the assessment of measured critical currents.

In order to compensate the thermal expansion during cooldown to operational temperature, a concept based on the reduction of the amplitude of sinusoidal arrangement of HTS CroCo strands along a cylinder barrel is proposed and investigated with respect to its electromechanical boundaries.

***Index Terms*— REBCO, 2G-HTS, busbar, DC power transmission, DC application**

I. Introduction to High Direct Current Applications

In industrial processes, an increasing number of applications are based on high direct currents (DC). In particular in electrolysis applications, direct currents ranging from the 10 kA range to up to 600 kA are used [1]-[5] with highest values in aluminum electrolysis plants [1]-[3].Steel production or recycling in electric DC arc furnaces are operated in the range of ~50 kA. [6],[7]. With increasing digitalization, the power consumption of data centers increases, and low-voltage DC system architectures are investigated with amperages in the 15-200 kA region, the amperage is largely depending on the system voltage of 48 V or 400 V [1],[2],[8],[9]. But also future mobility systems like DC railway grids [10] or cables in future electric airplanes [11], [12] or on board of large ships [13] may be operated around 5-10 kA. For the medium-voltage (MV) connection of large (off-shore) wind parks or MV-DC power transmission, system architectures with amperages ~10 kA were proposed [1], [14]. Similar amperages (~10 kA) were targeted in superconducting high voltage (HV) DC transmission lines [1], [15]. For the busbars of the magnet systems and busbars of future fusion magnets, currents in the 50-100 kA range are required [16],[17]. In high-energy physics research, different types of magnets need to be energized by high currents in the 10 kA range [18] and designs for future detector magnet systems aim at currents up to 80 kA [19],[20], also requiring busbars for these amperages.

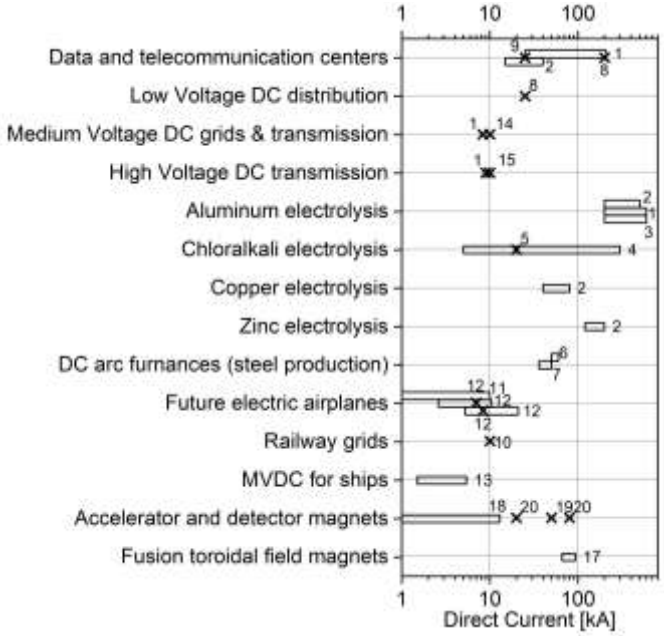

Fig. 1. High direct current (DC) applications.

II. Use of HTS in DC Applications

For most of the aforementioned high DC applications, solutions based on high temperature superconductor (HTS) were pro-

The project is funded by the German Federal Ministry for Economic Affairs and Climate Action under Grant No. 03ET1670.

(Corresponding author: Michael Wolf, e-mail: michael.wolf@kit.edu*)*

M. J. Wolf, W. H. Fietz, M. Heiduk, A. Kienzler, S. I. Schlachter, T. Vogel are with the Karlsruhe Institute of Technology (KIT), Institute for Technical Physics (ITEP), PO Box 3640, 76021 Karlsruhe, Germany.

S. Huwer is with Vision Electric Super Conductors GmbH, Morlauterer Str. 21, 67657 Kaiserslautern, Germany

Color versions of one or more of the figures in this paper are available online at http://ieeexplore.ieee.org.

Digital Object Identifier will be inserted here upon acceptance.

Template version 8.0d, 22 August 2017. IEEE will put copyright information in this area
See http://www.ieee.org/publications_standards/publications/rights/index.html for more information.

posed. In addition to a reduction of Ohmic losses, HTS solutions can generally be smaller and have lower weight due to the high current densities in HTS materials. The replacement of conventional aluminum busbars by a HTS solution in aluminum electrolysis was already proposed in 1995 [21]. The technical realization of HTS busbars of such high amperages is challenging and only few prototype HTS high current DC busbar systems were realized and operated so far including applications such as aluminum electrolysis [22], railway grids [23], chlorine electrolysis [24], and HV-DC transmission [15]. The amperage of realized HTS DC busbar systems remained at or below 20 kA. This is at least an order of magnitude below the typical operating current of state-of-the-art aluminum production plants as it can be seen from Fig. 1.

III. DEMO200 - Geometry, REBCO Properties and Design Process

The research project DEMO 200 aims to bridge this amperage gap and targets a modular 200 kA, liquid nitrogen (LN_2)-cooled DC busbar system, termed DEMO 200, for industrial electrolysis applications.

A. Geometry of the modular 200 kA busbar system

The 200 kA busbar is composed of ten modules of 20 kA to be operated in parallel. The arrangement and maximum dimensions of the 20 kA modules in the 200 kA busbar, and the design temperature were fixed at the beginning of the project (refer to [25] for details). Fig. 2(a) shows the cross-sectional schematics of the modular 200 kA busbar system. The ten modules with maximum lateral dimensions L_0 = 56 mm, are arranged in circular fashion (radius R_1 = 115 mm) at locations A, B, C, etc.. This arrangement allows the horizontal access to all ten modules, which is helpful for the assembly. An initial sub-scale test of a single module (Fig. 2(b)) at T = 77 K is planned prior to the assembly of the DEMO 200 busbar, the expected critical currents are calculated to allow for an assessment of measured critical currents. Within the project, several module designs based on different HTS assemblies are investigated (see [25] for details), this manuscript focuses on the specific arrangement based on HTS CroCo stands as shown in Fig. 2(b), and will be discussed in detail in chapter III.C.

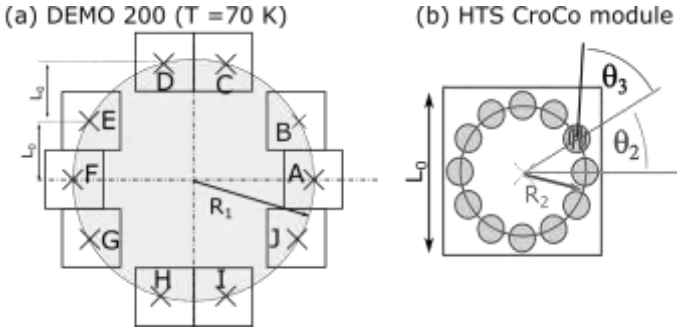

Fig. 2. (a) Cross-sectional schematics of the modular 200 kA busbar system. The busbar consists of 10 modules of 20 kA current carrying capacity with lateral dimensions L_0, = 56 mm whose centers are arranged in circular fashion (radius R_1 = 115 mm) at locations A, B, C, …. The DEMO 200 busbar will be operated at $T \leq 70$ K. (b) The 20 kA HTS CroCo modules discussed in this manuscript are formed from a circular arrangement (radius R_2) of a number n_{CroCo} HTS CroCo strands (grey circles) whose positions are given by θ_2. The angle θ_3 represents the orientation of the REBCO tapes (black lines) in the HTS CroCo strands. Figures are not to scale.

TABLE I
List of Parameters of the 200 kA Busbar System made from HTS CroCo Strands

Quantity	Value and Unit
Operational current I_{op}	200 kA
Number of modules	10
Max. Operational Temperature	70 K
R_1	115 mm
L_0	56 mm
R_2	20 mm
n_{CroCo}	12
d_{CroCo}	~ 3.8 mm
w_3	3 mm
w_2	2 mm
$n_{REBCO,\ 3mm}$	12
$n_{REBCO,\ 2mm}$	6
copper tape dimensions	2 mm x 0.1 mm 3 mm x 0.2 mm
$n_{Cu,3mm}$	5
$n_{Cu,2mm}$	4
REBCO tape thickness	80 µm
Solder thickness between tapes	10 µm

B. REBCO Tape Properties

The angular and field dependence of the critical current of the REBCO tapes is a key input parameter to the self-consistent electromagnetic calculation of the critical current of the busbar system. Therefore, measurements on a 2 mm wide tape, which will be used in the sub-scale test was characterized at both 70 K and 77 K to obtain data at temperatures and fields relevant to the 200 kA application at T ~ 70 K and the 77 K sub-scale test. Fig. 3 shows the angular and field dependence of the critical current of a 2 mm wide REBCO tape (symbols). The data is fit (solid lines) to an elliptical model:

$$I_c(B,\varphi) = I_{c0} \Big/ \left(1 + \sqrt{k^2 B_\parallel^2 + B_\perp^2}/B_c\right)^\beta \qquad (1)$$

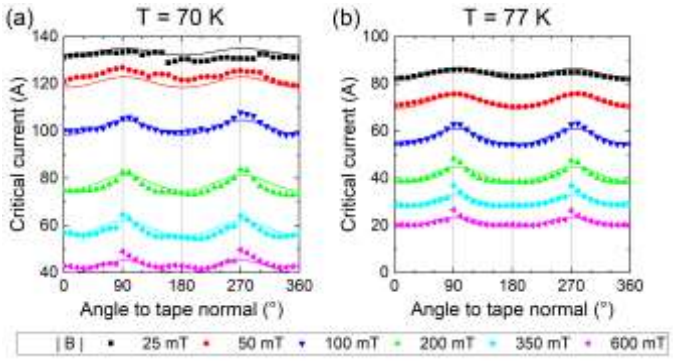

Fig. 3. Angular and field dependence of the critical current of a 2 mm wide REBCO tape (symbols) to be used in the sub-scale busbar demonstrator together with a fit of the data to eqn. (1) (solid lines). The obtained fitting parameters are listed in Table II. (a) Critical current at T = 70 K. The critical current at self-field conditions is I_c(70 K, sf) = 132 A. (b) Critical current at T = 77 K. The critical current at self-field conditions is I_c(77 K, sf) = 85-88 A.

TABLE II
LIST OF PARAMETERS OF THE REBCO TAPES OBTAINED FROM MEASUREMENTS SHOWN IN FIG. 2

Quantity	T = 70 K	T = 77 K
I_{c0}	75.09 A/mm	50.6 A/mm
B_c	0.14942 T	0.07828 T
θ_0	2.9°	3.6°
β	0.82296	0.7687
k	0.82291	0.74172
Measured $I_c(T, \mathrm{sf})$	132 A	85-88 A
Calculated $I_c(T, \mathrm{sf})$	135.6 A	89.8 A

from which the parameters I_{c0}, k, B_c and β are obtained. Additionally, an angle correction factor (θ_0) is used in the fit to account for misalignments of the experimental setup, therefore this parameter is not necessary in the calculations. The fitting parameters are listed in Table II.

The individual REBCO tape segments that will be used in the HTS CroCo modules of the sub-scale demonstrator have different critical currents. As many tapes from several individual pieces (but from the same order) will be connected in parallel, the length-weighted average of critical current of 2 mm and 3 mm wide REBCO tapes is used in calculations. In order to account for the difference in critical current to the measured 2 mm wide tape, a correction factor is applied for both tape types (Table III).

C. Design of the 20 kA module made from HTS CroCo strands

A rough estimate for the required amount of REBCO tapes for the 200 kA busbar can be obtained in the following way: An infinitely long conductor with current I_{op} leads at distance R_1 to a magnetic field of ~ 0.35 T. From the field dependence of the critical current (Fig. 2), one reads I_c (2mm, 70K, 0.35 T) ~ 60 A. Thus, one requires about 6 m REBCO width for the whole DEMO200 busbar.

In this work, the design of the 20 kA modules from so-called "HTS CroCo strands" is discussed. The HTS CroCo is a rigidly soldered stack of tapes of two different widths, with optimum width ratio w_2/w_3 ~ 0.618 and typically about twice the number of the wider tapes compared to the narrower tapes [26]. As bending and movement of the strands is required to compensate the thermal expansion during cooling (see chapter IV for details), HTS CroCos are formed from narrow REBCO tapes of w_3 = 3 mm and w_2 = 2 mm width. Starting with these assumptions, the number of HTS CroCos in the 20 kA modules (n_{CroCo}) and the number of REBCO tapes in the CroCos can be determined to achieve the required critical current.

TABLE III
LIST OF ELECTROMAGNETIC PARAMETERS OF THE REBCO TAPES USED IN THIS WORK

Quantity	w_1 = 3 mm	w_2 = 2 mm
Average I_c(77K, sf)	165.8 A	98.9 A
I_c-correction factor	1.2645	1.1145

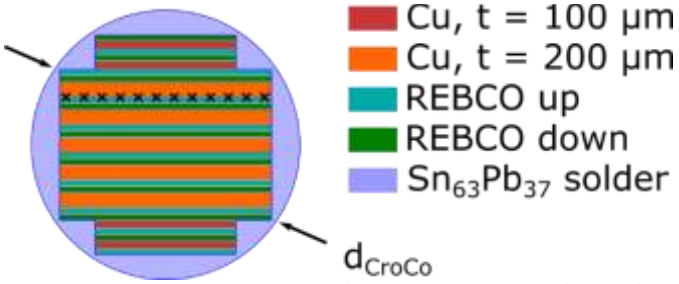

Fig. 4. Cross-sectional schematics of a HTS CroCo strand formed from REBCO and copper tapes of two different widths. The general layout is such that the REBCO sides of the REBCO tapes are facing towards a central copper tape. For one tape, the discretization of the tape into individual current-carrying wires is depicted by black crosses.

One choice is the use of twelve HTS CroCo strands each with twelve 3-mm- and six 2-mm-wide REBCO tapes, leading to 576 mm total REBCO width per module. If these HTS CroCos are arranged in a round shape (Fig. 2(b)) at radius R_2, the space between the HTS CroCos can be used for support structures and for current injection at the terminations.

Fig. 4 shows the cross-sectional schematics of these HTS CroCo strands, key parameters are listed in Table I. The general layout is such that the REBCO sides of the REBCO tapes are facing towards a central copper tape as this orientation was successfully fabricated and used in previous work [27].

IV. COMPENSATION OF THERMAL EXPANSION

In order to compensate the thermal expansion of the superconductor compared to elements of the busbar that remain at room temperature (e.g. outer cryostat walls), several methods can be applied, such as a compensation at the terminations [28], [29], arc-shaped bends [30], a radial movement of helically wound strands [31], or wave-like installations [32]. In this work, the HTS CroCo strands will be mechanically supported using support rings that can rotate on a central support. During

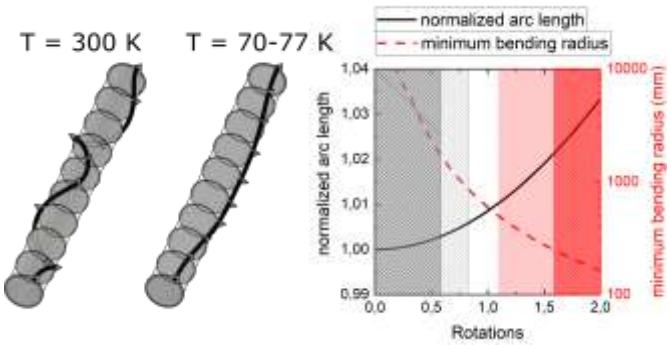

Fig. 5. The sketch (not to scale) to the left shows for one HTS CroCo of the module the concept for the compensation of thermal expansion by reducing the amplitude of a "wavy" HTS CroCo trajectory in a cylindrical arrangement. The plot on the right demonstrates the operational window to be realized in a 2.12 m-long sub-scale test which is determined from the competing requirements of having a sufficiently high arc length but at the same time a not too small bending radius.

preparation, the central support rings will be rotated and the required extra length of superconductor will be installed. During cooling, the wave-like structure stretches and the amplitude of the waves reduces (but should be > 0 to "guide" a subsequent warm-up). Therefore, the terminals can remain in a fixed orientation and thermal expansion will be compensated within the HTS CroCo module itself. Fig. 5 illustrates the concept, the left plot shows the system during installation, the right one at operational temperature. During the sub-scale test, in which 2.12 m long 20 kA modules will be tested, the concept will be investigated with the help of a mechanical support structure that prevents the axial movement of the terminations.

If one assumes that the HTS CroCo strands follow a sinusoidal trajectory along the cylinder barrel, one may calculate the effective arc length and determine the minimum number of rotations. Relevant materials for cryostat and cable assemblies such as stainless steel 304 or copper shorten by ~ 0.3 % upon cooling from room temperature to 70-77 K [33].

On the other hand, the tolerable bending radius of this type of HTS CroCo strands was determined in previous work to be ~250 mm [34]. As the bending radius decreases with the number of rotations, an upper limit of rotations can be determined.

Using calculus expressions for the arc length and curvature of a space curve, one obtains the viewgraph of Fig. 5. The dark areas indicate the maximum and minimum number of rotations, resulting from $\delta l/l > 0.003$ and $r_{bend} > 250$ mm, respectively, the pale areas consider a safety factor of 2. One can read from the graph that a rotation of the center of the sub-scale test module by 360° will satisfy both requirements and will therefore be targeted in the sub-scale test.

V. Calculation of Critical Currents

A. Modelling Approach

In order to calculate the electromagnetic performance of the 200 kA busbar, its voltage-current-characteristics needs to be calculated and $I_c > 200$ *kA* needs to be ensured.

The concept for the compensation of the thermal expansion may lead to helically wound HTS strands along the busbar axis at operation which will require special attention for modeling (unless a full 3D modelling approach is used). Two cases are therefore distinguished:

Case I assumes that the helical twist of the HTS CroCo modules is adjusted such that at operating conditions, the HTS CroCos are fully straightened. Then, a 2D-cross-sectional-calculation based on infinitely long straight conductors is suitable without any further adjustments.

Case II occurs if the HTS CroCo strands are "heavily overtwisted" such that at least one full rotation remains along the busbar axis at operating temperatures. Then each HTS CroCo comes at some position along the cable to the position, where its critical current is lowest, such that for the entire cable length all HTS CroCos of one module will show the same $E(I)$ characteristics. This condition can be enforced in a 2D-model by (artificially) adjusting the values I_{c0} in Eq. 1 until the same critical and operational current is obtained for all HTS CroCos of a given module.

The approach for obtaining the critical currents of the two cases is now as follows:

First, the superconducting layers are discretized into a number of straight, infinitely long current-carrying filaments with $I_c(B,\theta)$ dependence from Eq. (1) as described by Zermeno *et al.* in [35], [36] and orientation according to the normal vector of the tape. The filaments are assumed to be in an ideal parallel connection, i.e., have the same voltage difference, contact resistances are not considered here and will be discussed later (see chap. V.D). Along the current path, the voltage drop along each filament is modelled by the power-law electric field current dependence:

$$E\left(I_{op,i}\right) = E_c\left(I_{op,i}/I_c\left(B\left(I_{op,i}\right),\theta\right)\right)^n \qquad (2)$$

with $E_c = 10^{-4}$ V/m and $n = 15$.

After the discretization of the superconducting layers into an arrangement of straight current threads, the HTS properties (parameters of (1)) and the target electric field E are defined and all current carrying threads are initialized to operate at $I_{op,i} = I_{c0}$. Then, the magnetic field profile B_i is calculated from the $I_{op,i}$ distribution, followed by the critical current distribution $I_{c,i}$ of all threads according to (1). Finally, an updated $I_{op,i}$ can be obtained from (2).

These steps are repeated until $I_{op,i}$ changes less than a threshold compared to the previous iteration.

For Case I, the calculation is now completed and operational and critical currents of the modules and flux density plots can be calculated.

For Case II, the calculations of Case I have to be repeated until the critical current of all HTS CroCos of a given module, defined as sum of all constituting current threads, is equal. This is achieved by adjusting iteratively per module the I_{c0} values by the ratio of the minimum HTS CroCo critical current and the critical current of the corresponding HTS CroCo (while ensuring that I_{c0} is maintained for at least one HTS CroCo).

B. 200 kA busbar and DEMO 200 demonstrator (T = 70 K)

For a given electric field, the operational and critical current of the 200 kA busbar is calculated. Fig. 6 shows field plots of the 200 kA busbar at $E(I_{op}) = E_c = 100$ µV/m for both cases I (left column, $I_{op} = I_c = 240$ kA) and case II (right column, $I_{op} = I_c = 215$ kA). The configuration is for both cases $\theta_2 = n\times30°$ ($n = 1..12$), $\theta_3 = 0$, i.e., tapes are oriented radially. The plots (c) and (d) are zoom-ins to the module highlighted by a black box in (a) and (b). Black dots indicate the location of the current-carrying elements, white arrows indicate the field direction. Due to the fairly homogeneous arrangement of the ten modules in the busbar, the difference in operational currents among the modules is below 1%. This implies that the – from the superconductor's point of view, no substantial differences between the DEMO 200 demonstrator (series connection of modules) and the 200 kA busbar application (parallel connection of modules) is expected. It was calculated for case I that the orientation

of the tapes in the HTS CroCos (variation of θ_3 = 0°, 30°, 45°, 60°, 90°) at E~ 2.2 µV/m changes the total operational current by < 1 % which may be expected due to the fairly isotropic angular dependence of the critical currents of the REBCO tapes (Fig. 3).

The magnetic field profile across the 20 kA modules (Fig. 6(c), 6(d)) leads to a difference of $2\times(\max(I_c)-\min(I_c))/(\max(I_c)+\min(I_c))$ ~ 33% in the critical currents among the twelve HTS CroCos for the aforementioned parameters in case I as it is shown by black squares in Fig. 6(g). For θ_3 = 90°, the variation of the CroCo critical currents in case I is smallest, but still ~25%. For radially oriented tapes (θ_3=0°), several module

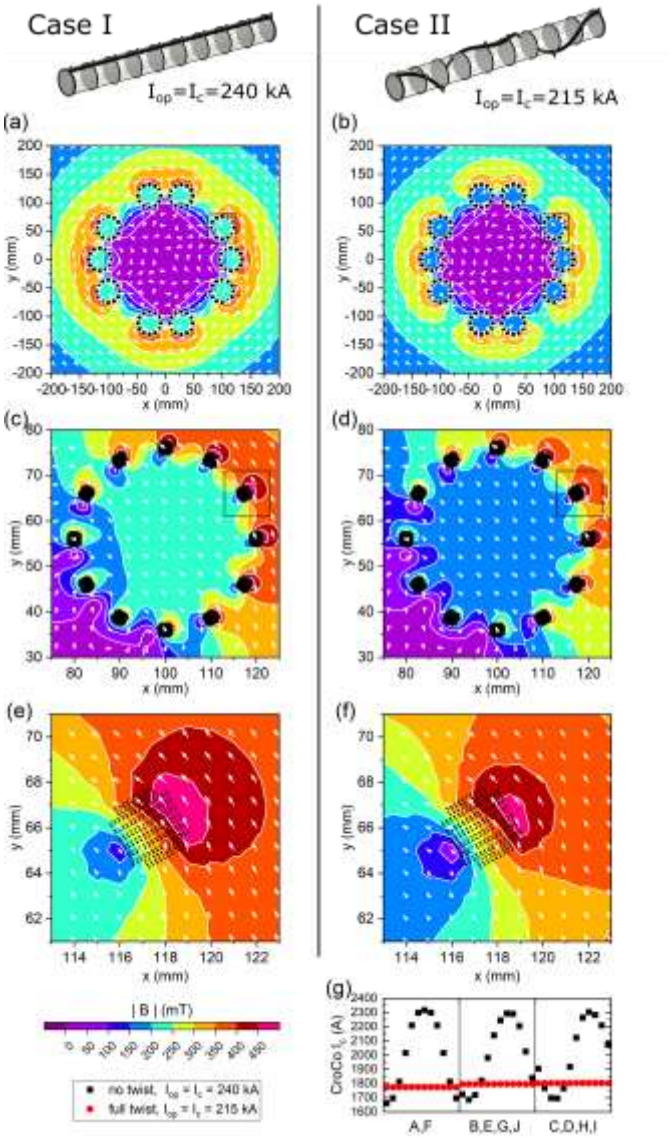

Fig. 6. Field plot of the DEMO200 busbar for both cases I (left column, panels (a),(c), and (e)) and case II (right column, panels (b),(d), and (f)) . The configuration is θ_2 = n×30° (n = 1..12), θ_3 = 0 (i.e., tapes are oriented radially in each module), T = 70 K. The color bar of the magnetic field magnitude at the bottom of the figure is valid for (a)-(f). The plots (c) and (d) are zoom-ins to the module highlighted by black boxes in (a) and (b) and to the HTS CroCos ((e) and (f)) as inducated in (c) and (d). Black dots indicate the location of the current-carrying elements, white arrows indicate the field direction. (g) shows the critical currents of the twelve HTS CroCos for the three types of positions of modules (Fig. 2(a)).

positions are electromagnetically equivalent, and only the three types of locations A,B,C have to be considered. The smallest critical current of all HTS CroCos in the busbar is 1.66 kA (θ_3 = 0°). For case II, a variation of the critical currents of the modules of 1.5 % is obtained with a lowest module critical current I_c = 21.3 kA corresponding to 1.77 kA for each CroCo of this module. These calculations show that the target critical current of 200 kA for the whole busbar is expected to be achieved, even in the more challenging twisted configuration of case II.

C. *Sub-scale test (T = 77 K).*

For the sub-scale testing, a single HTS CroCo module of 2.12 m length (inner length between the terminals) will be tested in a boiling nitrogen bath at T = 77 K. Here the cases I and II do not need to be distinguished as all HTS CroCos have the same critical current by symmetry. Fig. 7(a) shows a field plot of the sub-scale test setup (T = 77 K) where the module is operated at the critical electric field, (b) is a zoom-in to a single HTS CroCo. The configuration is θ_2 = n×30° (n = 1..12), θ_3 = 0° (i.e., tapes are oriented radially). The current in the module

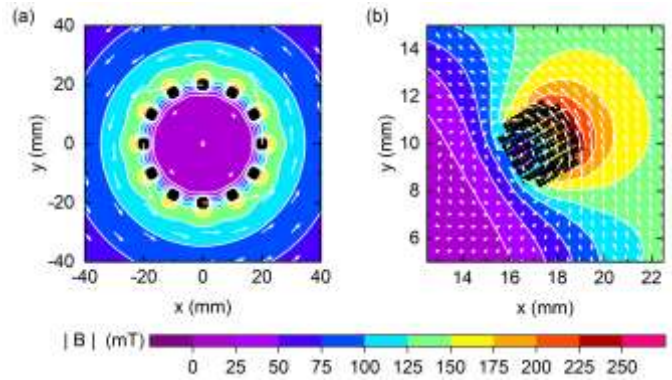

Fig. 7. (a) Field plot of the sub-scale test setup (T = 77 K) at the assumption that the module is operated at its critical current (E = 1 µV/cm). The configuration is $\theta_2 = n\times30°$ (n = 1..12), θ_3 = 0° (i.e., tapes are oriented radially). (b) Zoom-in to a single HTS CroCo strand.

is I_{op} = 17.3 kA

D. *Influence of contact-resistances*

Contact resistances are a key element of DC busbars and cables and were investigated by both modelling and experimental approaches [37]-[40]. In previous works on a 35 kA HTS CroCo – based multi-strand cable [41]-[44] of larger HTS CroCo strands made from 6- and 4-mm-wide tapes, contact resistances were both measured and modelled. In [44], a contact resistance variation (sum of both terminations) from 325 nΩ to 548 nΩ among 12 HTS CroCos was determined from a fit to the measured voltage-current-characteristics of a 35 kA demonstrator.

From these values, a contact resistance distribution R_{cont} = 422 +/- 66 nΩ is extracted. Contact resistances are considered by an additional linear $V(I) = R_{cont}\, I$ contribution to Eq. 2 and all HTS CroCos of a system are assumed to be in par-

allel connection. The influence of a modified current distribution on the I_c-distribution through the modified field profile is neglected.

If one compares for $I = I_c$(CroCo) the terminal voltages $V_{term}(I_c) = R_c\, I_c$ = 608 µV with the voltage along the superconductor $V_{HTS}\,(I_c) = E_c\, L$ = 212 µV, one immediately notices that $V_{term}(I_c) > V_{HTS}(I_c)$ for the short sub-scale demonstrator with L = 2.12 m, whereas for the 600-m-long target busbar application, the opposite is observed. Therefore, the influence of a contact resistance distribution is considered for the single-module, sub-scale case.

Fig. 8(a) shows the distribution of HTS CroCo currents of one module at 77 K as function of the module current for a contact resistance distribution R_{cont} = 422 +/- 66 nΩ. The dashed horizontal line marks the CroCo critical current, the vertical arrow indicate the module current, at which the first HTS CroCo reached its critical current. It is clearly visible, that the chosen contact resistance distribution leads to a spread of the critical currents. Panel (b) shows the statistical distribution of cable currents, at which the first HTS CroCo reached its I_c. 10,000 sets of contact resistance were calculated. A contact resistance

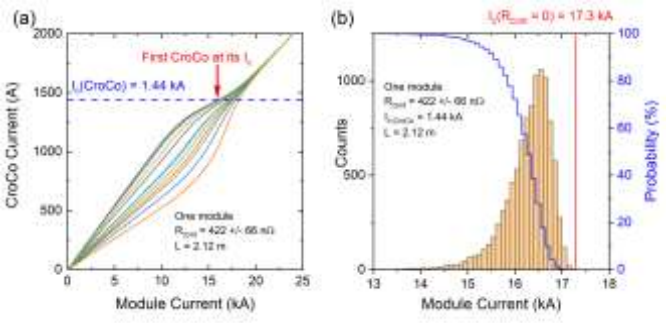

Fig. 8. (a) Distribution of HTS CroCo currents of one module at 77 K as function of the module current for a contact resistance distribution R_{cont} = 422 +/- 66 nΩ. The dashed horizontal line marks the CroCo critical current, the vertical arrow the module current, at which the first HTS CroCo reached its Ic. (b) Statistical distribution of cable currents, at which the first HTS CroCo reached its I_c for 10,000 sets of contact resistance.

distribution leads to a reduction of the critical currents. The 95% probability level is I_{cable} = 15.3 kA, i.e. a reduction by 2 kA compared to R_{cont} = 0.

VI. Conclusion

In this work the design and analysis of 20 kA modules made of HTS CroCo strands for a 200 kA busbar system is presented.

One key requirement that was not addressed in previous work of a superconducting busbar system is the availability of a concept for the compensation of the thermal expansion during cooling. It was calculated that by reducing the amplitude of a wave-like trajectory of HTS CroCo strands on a cylinder barrel, the expected thermal expansion can be compensated. If strands are helically twisted at operating conditions, the 2D modelling approach had to be adjusted to integrate this geometry as well. Calculations for two extreme cases (with and without helical twist) have shown that the helical twisting leads to a ~10% reduction of the critical current compared to the untwisted case, but that for the proposed configuration, the target critical current is still exceeded by 7.6 %.

Additionally, the influence of contact resistances on the current distribution and the total critical was investigated. Based on contact resistance values from previous work, it was calculated that for the planned sub-scale test, this contact resistance distribution will reduce the critical with 95% probability by ~12 %. For the target, 600-m-long application, contact resistances will not have a strong effect on the overall critical current, but tape homogeneity may become relevant here.

In the next phase of the project, HTS CroCo strands will be fabricated and the sub-scale test with a HTS CroCo module will be prepared.

Acknowledgment

The authors would like to thank B. Ringsdorf for performing the measurements of critical currents.

References

[1] A. Morandi, “HTS dc transmission and distribution: concepts, applications and benefits” *Supercond. Sci. Technol.* 28 (12), (2015), Art.ID. 123001

[2] W. Reiser, presented at ZIEHL V (2016), [Online]. Available: https://ivsupra.de/wp-content/uploads/2019/01/ZIEHL_V_2016_3_2_Industrie_Stromschienen_VESC_Reiser.pdf

[3] H. Kvande and P. A. Drabløs, "The Aluminum Smelting Process and Innovative Alternative Technologies," *Journal of Occupational and Environmental Medicine*, vol. 56, May 2014, pp. S23-S32.

[4] T. F. O’Brien, T. V, Bommaraju, F. Hine, *Handbook of Chlor-Alkali Technology*. Dordrecht : Springer, 2007, doi: 10.1007/b113786

[5] S. Elschner, presented at EUCAS (2017), [Online]. Available: https://indico.cern.ch/event/659554/contributions/2709494/attachments/1527269/2388459/3LO4-07_Steffen_Elschner_Room_1.pdf

[6] F. Qian, B. Farouk, and R. Mutharasan, “Modeling of Fluid Flow and Heat Transfer in the Plasma Region of the dc Electric Arc Furnace*” Metallurgical & Materials Transactions B,* vol. 26B, (Oct, 1995), pp. 1057ff.

[7] M. Ramírez, *et al.*, “Modeling of a DC Electric Arc Furnace—Mixing in the Bath” *ISIJ International*, vol. 41, no. 10, 2001, pp. 1146–1155.

[8] M. Furuse, S. Fuchino, N. Higuchi and I. Ishii, "Feasibility study of low-Voltage DC Superconducting distribution system," *IEEE Transactions on Applied Superconductivity*, vol. 15, no. 2, June 2005, pp. 1759-1762, doi: 10.1109/TASC.2005.849275

[9] J. V. Minervini, *et al.*, “Superconducting DC Power Transmission and Distribution: Final Report to the MIT Energy Council”, MIT PSFC (2009), [Online]. Available: https://dspace.mit.edu/bitstream/handle/1721.1/93303/09rr002_full.pdf;sequence=1

[10] M. Tomita *et al.*, *Journal of Applied Physics* vol. 111, 2012, Art. no. 063910.

[11] S. I. Schlachter *et al.*, presented at CEC-ICMC (2017), [Online]. Available: https://indico.cern.ch/event/578092/contributions/2537822/attachments/1491653/2345743/M2OrE-04_Schlachter.pdf

[12] M. Boll *et al.*, “A holistic system approach for short range passenger aircraft with cryogenic propulsion system”, *Supercond. Sci. Technol.*, vol. 33, 2020, Art.no. 044014.

[13] P. Cheetham, *et al.*, *IEEE Electric Ship Technologies Symposium*, 2019, pp. 548-555

[14] M. Noe and T. Arndt, “Superconductivity for green energy”, presented at EUCAS 2021

[15] C. E. Bruzek *et al*., "Cable Conductor Design for the High-Power MgB2 DC Superconducting Cable Project of BEST PATHS," *IEEE Transactions on Applied Superconductivity*, vol. 27, no. 4, June 2017, Art no. 4801405.

[16] V. Corato *et al*., "Progress in the design of the superconducting magnets for the EU DEMO", *Fusion Engineering and Design*, vol. 136 B, 2018, pp. 1597-1604.

[17] V. Corato *et al.*, "The DEMO Magnet System – Status and Future Challenges", *Fus. Eng. Des.*, vol. 174, Jan. 2022, Art. no. 112971.

[18] A. Ballarino, K. H. Meß and T. Taylor, "Extending the Use of HTS to Feeders in Superconducting Magnet Systems," *IEEE Transactions on Applied Superconductivity*, vol. 18, no. 2, June 2008, pp. 1455-1458.

[19] M. Mentink, A. Dudarev, T. Mulder, J. Van Nugteren and H. ten Kate, "Quench Protection of Very Large, 50-GJ-Class, and High-Temperature-Superconductor-Based Detector Magnets," *IEEE Transactions on Applied Superconductivity*, vol. 26, no. 4, June 2016, Art no. 4500608.

[20] M. Mentink *et al*., "Design of a 56-GJ Twin Solenoid and Dipoles Detector Magnet System for the Future Circular Collider," *IEEE Transactions on Applied Superconductivity*, vol. 26, no. 3, April 2016, Art no. 4003506.

[21] M. Runde, "Application of High-Tc superconductors in Aluminum Electrolysis Plants," *IEEE Trans. Appl. Supercond.*, vol. 5, no. 2, June 1995, pp. 813-816.

[22] D. Zhang *et al.*, "Stability Analysis of the Cable Core of a 10 kA HTS DC Power Cable Used in the Electrolytic Aluminum Industry," *IEEE Trans. Appl. Supercond.*, vol. 25, no. 3, June 2015, Art. no. 5402304.

[23] M. Tomita, M. Muralidhar, K. Suzuki, Y. Fukumoto and A. Ishiara, "Development of 10 kA high temperature superconducting power cable for railway systems," *J. Appl. Phys.*, vol. 111, no. 6, 2012, Art. no. 063910.

[24] S. Elschner, *et al*., "3S–Superconducting DC-Busbar for High Current Applications," *IEEE Trans. Appl. Supercond.*, vol. 28, no. 4, 2018, Art. no. 4800805.

[25] S. Elschner et al., "DEMO200 concept and design of superconducting 200 kA DC busbar demonstrator for application in an aluminum smelter", presented at EUCAS 2021, submitted to *IEEE Trans. Appl. Supercond*.

[26] M. J. Wolf, W. H. Fietz, C. M. Bayer, S. I. Schlachter, R. Heller and K. Weiss, "HTS CroCo: A Stacked HTS Conductor Optimized for High Currents and Long-Length Production," in *IEEE Transactions on Applied Superconductivity*, vol. 26, no. 2, March 2016, Art no. 6400106.

[27] D. S. Nickel, M. J. Wolf, K. Weiss and W. H. Fietz, "Mechanical and Electro-Mechanical Investigations of Assembled HTS CroCo Triplets," *IEEE Transactions on Applied Superconductivity*, vol. 30, no. 4, June 2020, Art no. 8400705.

[28] "Cable end" European Patent EP1617537A2.

[29] F. Schmidt, J. Maguire, T. Welsh, S. Bratt, "Operation Experience and further Development of a High-Temperature Superconducting Power Cable in the Long Island Power Authority Grid", *Physics Procedia*, vol. 36, 2012, pp. 1137-1144.

[30] Device for compensating for changes in length in superconductor cables European patent EP2589849A1.

[31] M. Takayasu, L. Chiesa, L. Bromberg and J. V. Minervini, "Electrical and Mechanical Characteristics of HTS Twisted Stacked-Tape Cable Conductor," *IEEE Transactions on Applied Superconductivity*, vol. 27, no. 4, June 2017, Art no. 6900305.

[32] S. Elschner *et al*., "3S–Superconducting DC-Busbar for High Current Applications," *IEEE Transactions on Applied Superconductivity*, vol. 28, no. 4, June 2018, Art no. 4800805.

[33] J. W. Ekin, "Experimental techniques for low-temperature measurements : cryostat design, material properties, and superconductor critical-current testing", Oxford Univ. Press, 2006.

[34] D. S. Nickel, W. H. Fietz, K. -P. Weiss and M. J. Wolf, "Impact of Bending on the Critical Current of HTS CrossConductors," *IEEE Transactions on Applied Superconductivity*, vol. 31, no. 5, Aug. 2021, Art no. 4603604.

[35] V. Zermeño *et al.*, "A self-consistent model for estimating the critical current of superconducting devices" *Supercond. Sci. Technol.*, vol. 28**,** 2015, Art. no. 085004.

[36] V. M. R. Zermeño, S. Quaiyum, F. Grilli: "Open Source Codes for Computing the Critical Current of Superconducting Devices" [Online]. Available: : http://arxiv.org/ftp/arxiv/papers/1509/1509.01856.pdf

[37] V. Zermeno *et al:* "Modeling and simulation of termination resistances in superconducting cables" *Supercond. Sci. Technol.*, vol. 27, 2014, Art. no. 124013.

[38] G. De Marzi *et al*: "Experimental and numerical studies on current distribution in stacks of HTS tapes for cable-in-conduit-conductors" *Supercond. Sci. Technol.*, vol. 34, 2021, Art. no. 035016.

[39] V. Pothavajhala, L. Graber, C. H. Kim and S. Pamidi, "Experimental and Model Based Studies on Current Distribution in Superconducting DC Cables," *IEEE Transactions on Applied Superconductivity*, vol. 24, no. 3, June 2014, Art no. 4800505.

[40] T. Mulder, A. Dudarev, M. Mentink, M. Dhallé and H. ten Kate, "Development of Joint Terminals for a New Six-Around-One ReBCO-CORC Cable-in-Conduit Conductor Rated 45 kA at 10 T/4 K," *IEEE Transactions on Applied Superconductivity*, vol. 26, no. 3, April 2016, Art no. 4801704.

[41] A. Preuß, "*Development of high-temperature superconductor cables for high direct current applications*", PhD thesis, KIT scientific publishing, 2021, doi: 10.5445/KSP/1000122861

[42] K.-P. Weiss, W. H. Fietz, M. Heiduk, C. Lange, A. Preuß and M. J. Wolf, "Development and test of a 35 kA-HTS CroCo cable demonstrator", *Journal of Physics: Conference Series* vol. 1559, no. 1, 2020, Art. no. 012082.

[43] M. J. Wolf, *et al.*, "HTS CroCo - A Strand for High Direct Current Applications", *Journal of Physics: Conference Series, vol.* 1590, no. 1, Art. no. 012020.

[44] M. J. Wolf, W. H. Fietz, M. Heiduk, C. Lange and K. -P. Weiss, "Current Redistribution in a Superconducting Multi-Strand 35 kA DC Cable Demonstrator," *IEEE Transactions on Applied Superconductivity*, vol. 31, no. 5, Aug. 2021, Art no. 4801505.